Iranian Journal of Fuzzy Systems

Volume 22, Number 2, (2025), pp. 25-39

Original paper

University of Sistan and Baluchestan

Application of combining type-2 fuzzy CMAC network and Jordan neural network in nonlinear system control

T. L. Le[1] and N. K. Long[2]

[1,2] *Faculty of Mechatronics and Electronics, Lac Hong University, Dong Nai, Vietnam*

tienloc@lhu.edu.vn, ngokimlong@lhu.edu.vn

Abstract

This paper proposes a new solution for controlling complex nonlinear systems, through the combination of a type-2 fuzzy CMAC controller and Jordan neural network. This method takes advantage of type-2 fuzzy CMAC in dealing with uncertainties and learning ability, while the Jordan neural network helps to enhance the stability and improve the performance of the system. The adaptive learning laws were designed to help the proposed network automatically update the network parameters. The results from simulations and experiments have shown that this method achieves superior accuracy and robustness compared to other methods. When applied to control the Magnetic Levitation System, this method shows great potential in solving complex nonlinear control problems, opening up new approaches in this field.

Keywords: Cerebellar model articulation controller, type-2 fuzzy system, Jordan neural network, adaptive control system.

1 Introduction

Cerebellar Model Articulation Controller (CMAC) is a control method based on the cerebellum model, commonly used in nonlinear control systems and machine learning. CMAC has strong learning and prediction capabilities thanks to its distributed neural network structure [2]. A popular variant of CMAC is Fuzzy CMAC, in which fuzzy rules are incorporated to enhance the ability to handle imprecise and uncertain information [5]. Although Fuzzy CMAC using Type-1 fuzzy has achieved many positive results in control applications, it still has difficulty in thoroughly handling the uncertainties and fluctuations of the system [16]. This is because type-1 fuzzy can only describe variables with a certain degree of uncertainty. To overcome this drawback, type-2 Fuzzy CMAC (T2FCMAC) is introduced, with the ability to better handle uncertainties through the use of Type-2 fuzzy sets. Type-2 fuzzy sets include not only the degree of membership but also the uncertainty about that degree of membership, which improves control efficiency [4]. Typical research works on type-2 fuzzy logic focus on solving uncertain and complex problems in many fields. Some studies have successfully applied type-2 fuzzy in the control of robotic systems, motor systems, and industrial applications, thanks to its ability to handle fuzzy and uncertain information better than type-1 fuzzy logic [3, 8, 11, 12, 15, 20, 27, 28]. In addition, type-2 fuzzy is also used in pattern recognition, signal processing, and control system optimization to improve accuracy and adaptability in a changing environment [9, 10, 17, 22, 25]. Improvements in methods such as type-2 fuzzy neural networks and advanced fuzzy control systems have also contributed to the development of this field. Jordan Neural Network (JNN) is a type of recurrent neural network capable of remembering the previous state of the system, thereby improving the stability and efficiency of the control system [4]. The JNN uses feedback loops to store information from previous steps, helping it better handle problems related to time series and dynamic states [14]. Recently, some notable studies using JNN networks include: In 2020, Su and Lin proposed a method using Jordan neural networks and the least squares algorithm to estimate weak signals in chaotic noise, the results showed that this method outperformed

Corresponding Author: T. L. Le
Received: December 2024; Revised: March 2025; Accepted: April 2025.
https://doi.org/10.22111/ijfs.2025.50552.8930

traditional methods in terms of accuracy and signal-to-noise ratio [24]. In 2021, Das et. al provided modeling of the electron beam welding process using Elman and Jordan recurrent neural network, optimized by algorithms such as search, the results showed that Jordan model optimized by flower pollination gave the best results [6]. In 2021, Kumari et. al proposed a convolutional Elman Jordan neural network, which uses small attention windows for image recognition, improving reconstruction and classification efficiency compared to previous methods [14]. Magnetic Levitation System is a common application in transportation, robotics, and industrial equipment fields [1]. This system uses magnetic force to lift and hold objects in a fixed position in space, without requiring physical contact. Controlling a magnetic ball lifting system is a major challenge due to the nonlinearity, hysteresis, and uncertainty of the system [30]. Current control methods for magnetic ball lifting systems include proportional-integral-derived (PID) control, fuzzy control, and modern control techniques such as predictive control, adaptive control, and optimal control [7, 13, 19, 21, 23, 26, 29, 31]. Although these methods have achieved much success, there are still limitations in terms of accuracy and resilience to system uncertainties and fluctuations. In this study, we combine the JNN with the T2FCMAC structure to create a new proposed controller. This combination is intended to take advantage of the T2FCMAC 's uncertainty handling and learning capabilities along with the state memory capabilities and high stability of the Jordan network. This research contributes a new control method for nonlinear systems, by combining two advanced technologies: T2FCMAC and JNN. The novelty of the research is to take advantage of the advantages of both technologies to improve control efficiency under uncertain and fluctuating conditions. Experimental results show that the proposed method not only improves accuracy but also improves system sustainability compared to traditional control methods.

2 The proposed T2FJCMAC Controller

In this section, the T2FCMAC method combined with JNN is designed to improve the control efficiency of nonlinear systems by taking advantage of both techniques. The developed T2FJCMAC network architecture is shown in Fig.1. The detailed description of its structure and operation is given as follows:

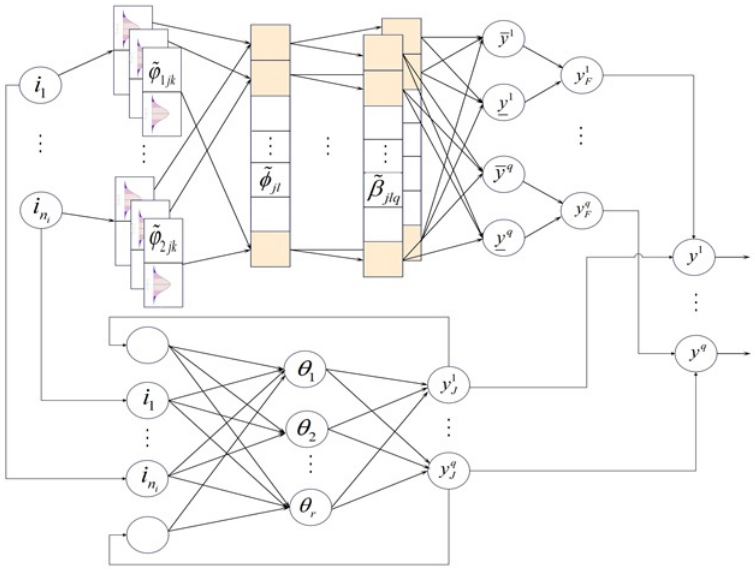


Figure 1: The developed T2FJCMAC network architecture.

2.1 Structure of T2FCMAC:

• **Input space:** this space contains the system input, which can be represented by state variables $\boldsymbol{I} = [i_1, i_2, \ldots, i_i, \ldots, i_{n_i}]$, where i_i is the i^{th} input.

• **Membership function space:** These fuzzy sets include the upper membership function (UMF) and lower membership function (LMF), representing each input variable's membership degree. This study uses the Type-2 Gaussian membership function, which can be given as:

$$\bar{\varphi}_{ijk} = \exp\left(-\frac{(i_i - o_{ijk})^2}{\bar{\nu}_{ijk}^2}\right), \tag{1}$$

$$\underline{\varphi}_{ijk} = \exp\left(-\frac{(i_i - o_{ijk})^2}{\underline{\nu}_{ijk}^2}\right), \tag{2}$$

where $\bar{\varphi}_{ijk}$ and $\underline{\varphi}_{ijk}$ are the UMF and LMF, respectively; o_{ijk} and $\bar{\nu}_{ijk}$, $\underline{\nu}_{ijk}$ are the mean and the standard deviations, respectively.

• **Fuzzy firing space:** This space creates the fuzzy inferences from input fuzzy sets LMF and UMF. These rules determine how the input variables affect the output control variables.

$$\bar{\phi}_{jl} = \prod_{i=1}^{n_i} \bar{\varphi}_{ijk}, \tag{3}$$

$$\underline{\phi}_{jl} = \prod_{i=1}^{n_i} \underline{\varphi}_{ijk}, \tag{4}$$

where $\bar{\phi}_{jl}$ and $\underline{\phi}_{jl}$ are the upper and lower fuzzy firing strengths.

• **Connecting weight space:** This space stores and adjusts the connection weights between the fuzzy firing space and the output space. These weights are learned through control and feedback to optimize control efficiency. It can be represented as follows:

$$\begin{bmatrix} \bar{\beta}_1 \\ \bar{\beta}_2 \\ \vdots \\ \bar{\beta}_{n_q} \end{bmatrix} = \begin{bmatrix} \bar{\beta}_{111}\cdots\bar{\beta}_{1n_l1}, & \bar{\beta}_{211}\cdots\bar{\beta}_{2n_l1}, & \cdots, & \bar{\beta}_{n_j11}\cdots\bar{\beta}_{njn_l1} \\ \bar{\beta}_{112}\cdots\bar{\beta}_{1n_l2}, & \bar{\beta}_{212}\cdots\bar{\beta}_{2n_l2}, & \cdots, & \bar{\beta}_{n_j12}\cdots\bar{\beta}_{njn_l2} \\ \vdots & \vdots & \ddots & \vdots \\ \bar{\beta}_{11n_q}\cdots\bar{\beta}_{1n_ln_q}, & \bar{\beta}_{21n_q}\cdots\bar{\beta}_{2n_ln_q}, & \cdots, & \bar{\beta}_{n_j1n_q}\cdots\bar{\beta}_{n_jn_ln_q} \end{bmatrix}, \tag{5}$$

$$\begin{bmatrix} \underline{\beta}_1 \\ \underline{\beta}_2 \\ \vdots \\ \underline{\beta}_{n_q} \end{bmatrix} = \begin{bmatrix} \underline{\beta}_{111}\cdots\underline{\beta}_{1n_l1}, & \underline{\beta}_{211}\cdots\underline{\beta}_{2n_l1}, & \cdots, & \underline{\beta}_{n_j11}\cdots\underline{\beta}_{njn_l1} \\ \underline{\beta}_{112}\cdots\underline{\beta}_{1n_l2}, & \underline{\beta}_{212}\cdots\underline{\beta}_{2n_l2}, & \cdots, & \underline{\beta}_{n_j12}\cdots\underline{\beta}_{njn_l2} \\ \vdots & \vdots & \ddots & \vdots \\ \underline{\beta}_{11n_q}\cdots\underline{\beta}_{1n_ln_q}, & \underline{\beta}_{21n_q}\cdots\underline{\beta}_{2n_ln_q}, & \cdots, & \underline{\beta}_{n_j1n_q}\cdots\underline{\beta}_{n_jn_ln_q} \end{bmatrix}, \tag{6}$$

where $\bar{\beta}_{jlq}$ and $\underline{\beta}_{jlq}$ are the upper and lower fuzzy connecting weights.

• **Output space:** In this space, the results from fuzzy firing space and connecting weight space are aggregated to create the system output.

$$y_{T2FCMAC}^q = \overline{y}_{T2FCMAC}^q + \underline{y}_{T2FCMAC}^q = \frac{1}{2}\sum_{j=1}^{n_j}\left(\frac{\sum_{l=1}^{n_l}\left(\overline{\phi}_{jl}\overline{\beta}_{jlq}\right)}{\sum_{l=1}^{n_l}\overline{\phi}_{jl}} + \frac{\sum_{l=1}^{n_l}\left(\underline{\phi}_{jl}\underline{\beta}_{jlq}\right)}{\sum_{l=1}^{n_l}\underline{\phi}_{jl}}\right). \tag{7}$$

2.2 Structure of Jordan neural network:

• **JNN Input space:** Receives state variables from the input space of T2FCMAC and the feedback from the JNN output space. By having a feedback loop that helps store and process information from previous steps.

$$\boldsymbol{\lambda} = [i_1, i_2, \ldots, i_i, \ldots, i_{n_i}, y_{JNN}^1, y_{JNN}^2, \ldots, y_{JNN}^q, \ldots, y_{JNN}^{n_q}] = [\lambda_1, \lambda_2, \ldots, \lambda_r, \ldots, \lambda_{n_r}], \tag{8}$$

where λ_r is the r^{th} input; y_{JNN}^q is the q^{th} feedback output of the JNN.

• **JNN hidden space:** The outputs from this space can be determined using the input space of the JNN and the associated hidden weights, γ_{mr}, as follows:

$$\theta_r = \sum_{r=1}^{n_r} \lambda_r \gamma_{mr}. \tag{9}$$

• **JNN output space:** The outputs of this space can be derived using the hidden layer of the JNN and the corresponding output weights, ω_{qr}, as follows:

$$y_{NN}^{q} = \sum_{r=1}^{n_r} \theta_r \omega_{qr}. \tag{10}$$

The final output of the proposed T2FJCMAC can then be obtained by combining the JNN output space with the T2FCMAC output space as follows:

$$y_{T2FJCMAC}^{q} = y_{T2FCMAC}^{q} + y_{NN}^{q}. \tag{11}$$

3 The parameter adaptation laws for T2FJCMAC Controller

To improve the tracking performance, this study employs high-order sliding mode techniques [18].

$$\begin{aligned} s(t) &= \sum_{p=0}^{p-1} \frac{(m-1)!}{p!(m-p-1)!} \left(\frac{\partial}{\partial t}\right)^{m-p-1} \gamma^p e \\ &= e^{(m-1)} + (m-1)\gamma e^{(m-2)} + (m-2)\gamma^2 e^{(m-3)} + \cdots + \gamma^{(m-1)} e, \end{aligned} \tag{12}$$

where γ is a positive constant that characterizes the slope of the sliding surface.
By differentiating equation (12)

$$\begin{aligned} \dot{s}(t) &= e^m + (m-1)\gamma e^{(m-1)} + (m-2)\gamma^2 e^{(m-2)} + \cdots + \gamma^{(m-1)} \dot{e} \\ &= \boldsymbol{e}^m + \boldsymbol{\gamma}^T \boldsymbol{e}, \end{aligned} \tag{13}$$

where $\boldsymbol{\gamma} = \left[(m-1)\gamma, (m-2)\gamma^2, \ldots, \gamma^{(m-1)}\right]^T \in \mathbb{R}^{m-1}$ denotes a positive gain vector. If m and γ are chosen to match the coefficients of a Hurwitz polynomial, then $\lim_{t\to\infty} e(t) = 0$. The Lyapunov cost function is defined as

$$V_1(s(t)) = \frac{1}{2}\left(s(t)\right)^2, \tag{14}$$

then

$$\dot{V}_1(s(t)) = s(t)\dot{s}(t). \tag{15}$$

An online learning gradient descent algorithm is applied to minimize $\dot{V}_1(s(k))$. Therefore, the online tuning for parameter adaptation laws of the proposed T2FJCMAC controller are given by the following equations:

$$\bar{\phi}_{jlq}(t+1) = \bar{\phi}_{jlq}(t) - \eta_\phi \frac{\partial s(t)\dot{s}(t)}{\partial \bar{\phi}_{jlq}} = \bar{\phi}_{jlq}(t) - \eta_\phi \frac{\partial s(t)\dot{s}(t)}{\partial Y_{T2FCAMC}^{q}} \frac{\partial y_{T2FCMAC}^{q}}{\partial \bar{y}_{T2FCMAC}^{q}} \frac{\partial \bar{y}_{T2FCMAC}^{q}}{\partial \bar{\phi}_{jlq}} = \bar{\phi}_{jlq}(t) - \frac{1}{2}\eta_\phi s(t) \sum_{j=1}^{n_j} \frac{\bar{\beta}_{jlq}}{\sum_{l=1}^{n_j} \bar{\beta}_{jlq}}, \tag{16}$$

$$\underline{\phi}_{jlq}(t+1) = \underline{\phi}_{jlq}(t) - \eta_\phi \frac{\partial s(t)\dot{s}(t)}{\partial \underline{\phi}_{jlq}} = \underline{\phi}_{jlq}(t) - \eta_\phi \frac{\partial s(t)\dot{s}(t)}{\partial Y_{T2FCAMC}^{q}} \frac{\partial y_{T2FCMAC}^{q}}{\partial \underline{y}_{T2FCMAC}^{q}} \frac{\partial \underline{y}_{T2FCMAC}^{q}}{\partial \underline{\phi}_{jlq}} = \underline{\phi}_{jlq}(t) - \frac{1}{2}\eta_\phi s(t) \sum_{j=1}^{n_j} \frac{\underline{\beta}_{jlq}}{\sum_{l=1}^{n_j} \underline{\beta}_{jlq}}. \tag{17}$$

$$\begin{aligned} o_{ijk}(t+1) &= o_{ijk}(t) - \eta_o \frac{\partial s(t)\dot{s}(t)}{\partial o_{ijk}} \\ &= o_{ijk}(t) - \eta_o \frac{\partial s(t)\dot{s}(t)}{\partial Y_{T2FCAMC}^{q}} \left(\frac{\partial y_{T2FCMAC}^{q}}{\partial \bar{y}_{T2FCMAC}^{q}} \frac{\partial \bar{y}_{T2FCMAC}^{q}}{\partial \bar{\phi}_{jl}} \frac{\partial \bar{\phi}_{jl}}{\partial \bar{\varphi}_{ijk}} \frac{\partial \bar{\varphi}_{ijk}}{\partial o_{ijk}} + \frac{\partial y_{T2FCMAC}^{q}}{\partial \underline{y}_{T2FCMAC}^{q}} \frac{\partial \underline{y}_{T2FCMAC}^{q}}{\partial \underline{\phi}_{jl}} \frac{\partial \underline{\phi}_{jl}}{\partial \underline{\varphi}_{ijk}} \frac{\partial \underline{\varphi}_{ijk}}{\partial o_{ijk}} \right) \\ &= o_{ijk}(t) - \frac{1}{2}\eta_o s(t) \left(\frac{\underline{\beta}_{jlq}(\underline{\phi}_{jlq} - \underline{y}_{T2FCMAC}^{q})}{\sum_{l=1}^{n_j} \underline{\beta}_{jlq}} \left(\frac{(i_i - o_{ijk})}{\underline{\nu}_{ijk}^2} \right) + \frac{\bar{\beta}_{jlq}(\bar{\phi}_{jlq} - \bar{y}_{T2FCMAC}^{q})}{\sum_{l=1}^{n_j} \bar{\beta}_{jlq}} \left(\frac{(i_i - o_{ijk})}{\bar{\nu}_{ijk}^2} \right) \right). \end{aligned} \tag{18}$$

$$\begin{aligned}\bar{\nu}_{ijk}(t+1) &= \bar{\nu}_{ijk}(t) - \eta_\nu \frac{\partial s(t)\dot{s}(t)}{\partial \bar{\nu}_{ijk}} \\ &= \bar{\nu}_{ijk}(t) - \eta_\nu \frac{\partial s(t)\dot{s}(t)}{\partial y^q_{T2FCMAC}} \frac{\partial y^q_{T2FCMAC}}{\partial \bar{y}^q_{T2FCMAC}} \frac{\partial \bar{y}^q_{T2FCMAC}}{\partial \bar{\phi}_{jl}} \frac{\partial \bar{\phi}_{jl}}{\partial \bar{\varphi}_{ijk}} \frac{\partial \bar{\varphi}_{ijk}}{\partial \bar{\nu}_{ijk}} \\ &= \bar{\nu}_{ijk}(t) - \frac{1}{2}\eta_\nu s(t) \left(\frac{\bar{\beta}_{jlq}(\bar{\phi}_{jlq} - \bar{y}^q_{T2FCMAC})}{\sum_{l=1}^{n_j} \bar{\beta}_{jlq}} \left(\frac{(i_i - o_{ijk})^2}{\bar{\nu}^3_{ijk}} \right) \right). \end{aligned} \tag{19}$$

$$\begin{aligned}\underline{\nu}_{ijk}(t+1) &= \underline{\nu}_{ijk}(t) - \eta_\nu \frac{\partial s(t)\dot{s}(t)}{\partial \underline{\nu}_{ijk}} \\ &= \underline{\nu}_{ijk}(t) - \eta_\nu \frac{\partial s(t)\dot{s}(t)}{\partial y^q_{T2FCMAC}} \frac{\partial y^q_{T2FCMAC}}{\partial \underline{y}^q_{T2FCMAC}} \frac{\partial \underline{y}^q_{T2FCMAC}}{\partial \underline{\phi}_{jl}} \frac{\partial \underline{\phi}_{jl}}{\partial \underline{\varphi}_{ijk}} \frac{\partial \underline{\varphi}_{ijk}}{\partial \underline{\nu}_{ijk}} \\ &= \underline{\nu}_{ijk}(t) - \frac{1}{2}\eta_\nu s(t) \left(\frac{\underline{\beta}_{jlq}(\underline{\phi}_{jlq} - \underline{y}^q_{T2FCMAC})}{\sum_{l=1}^{n_j} \underline{\beta}_{jlq}} \left(\frac{(i_i - o_{ijk})^2}{\underline{\nu}^3_{ijk}} \right) \right). \end{aligned} \tag{20}$$

$$\begin{aligned}\omega_{qr}(t+1) &= \omega_{qr}(t) - \eta_\omega \frac{\partial s(t)\dot{s}(t)}{\partial \omega_{qr}} \\ &= \omega_{qr}(t) - \eta_\omega \frac{\partial s(t)}{\partial y^g_{T2FJCMAC}} \frac{\partial y^g_{T2FJCMAC}}{\partial y^g_{JNN}} \frac{\partial y^g_{JNN}}{\partial \omega_{qr}} \\ &= \omega_{qr}(t) - \frac{1}{2}\eta_\omega s(t)\theta_r. \end{aligned} \tag{21}$$

$$\begin{aligned}\gamma_{mr}(t+1) &= \gamma_{mr}(t) - \eta_\gamma \frac{\partial s(t)\dot{s}(t)}{\partial \gamma_{mr}} \\ &= \gamma_{mr}(t) - \eta_\gamma \frac{\partial s(t)\dot{s}(t)}{\partial y^q_{T2FJCMAC}} \frac{\partial y^q_{T2FJCMAC}}{\partial y^q_{JNN}} \frac{\partial y^q_{JNN}}{\partial \theta_r} \frac{\partial \theta_r}{\partial \gamma_{mr}} \\ &= \gamma_{mr}(t) - \frac{1}{2}\eta_\gamma s(t)\omega_{qr}\lambda_r, \end{aligned} \tag{22}$$

where the derivative terms $\frac{\partial y^q_{T2FJCMAC}}{\partial \underline{y}^q_{T2FJCMAC}}$, $\frac{\partial y^q_{T2FJCMAC}}{\partial \bar{y}^q_{T2FJCMAC}}$, and $\frac{\partial s(t)\dot{s}(t)}{\partial y^q_{T2FJCMAC}}$ in (16)-(22) can be explained as:

$$\frac{\partial s(t)\dot{s}(t)}{\partial y^q_{T2FJCMAC}} = \frac{\partial s(t)(e^m + \boldsymbol{\gamma}^T \boldsymbol{e})}{\partial y^q_{T2FJCMAC}} = \frac{\partial s(t)(e^m + \boldsymbol{\gamma}^T e)}{\partial y^q_{T2FJCMAC}} = \frac{\partial s(t)(y^q_{T2FJCMAC} - y^q_{T2FJCMAC} + \boldsymbol{\gamma}^T \boldsymbol{e})}{\partial y^q_{T2FJCMAC}}. \tag{23}$$

$$\frac{\partial y^q_{T2FJCMAC}}{\partial \underline{y}^q_{T2FJCMAC}} = \frac{\partial(\overline{y}^q_{T2FJCMAC} + \underline{y}^q_{T2FJCMAC})}{\partial \underline{y}^g_{T2FJCMAC}} = 1. \tag{24}$$

$$\frac{\partial y^q_{T2FJCMAC}}{\partial \bar{y}^q_{T2FJCMAC}} = \frac{\partial(\overline{y}^q_{T2FJCMAC} + \underline{y}^q_{T2FJCMAC})}{\partial \bar{y}^g_{T2FJCMAC}} = 1. \tag{25}$$

In (24), because $\lim_{t\to\infty} e(t) = 0$ then:

$$\frac{\partial s(t)\dot{s}(t)}{\partial y^q_{T2FCAMC}} = \frac{\partial s(t)\left(e^m + \boldsymbol{\gamma}^T \boldsymbol{e}\right)}{\partial y^q_{T2FCMAC}} = \frac{s(t)\partial e^m + s(t)\partial \boldsymbol{\gamma}^T \boldsymbol{e}}{\partial y^q_{T2FCMAC}} = \frac{s(t)\partial\left(y^q_{T2FCMAC} - y^d_{T2FCMAC}\right) + s(t)\partial \boldsymbol{\gamma}^T \boldsymbol{e}}{\partial y^q_{T2FCMAC}} = s(t), \tag{26}$$

where $y^d_{T2FCMAC}$ is the desired value of $y^q_{T2FCMAC}$

Proof. First, defined:

$$\boldsymbol{F}_{\boldsymbol{\Theta}}(t) = \frac{\partial y^q_{T2FCMAC}}{\partial \boldsymbol{\Theta}}, \tag{27}$$

where $\boldsymbol{\Theta}$ is expressed in terms of $\bar{\phi}$, $\underline{\phi}$, o, $\bar{\nu}$, $\underline{\nu}$, ω, and γ in (16)-(22).
Utilizing the gradient descent technique for (16), obtained:

$$\dot{V}(s(t+1)) = \dot{V}(s(t)) + \Delta\dot{V}(s(t)) \approx \dot{V}(s(t)) + \left[\frac{\partial \dot{V}(s(t))}{\partial \boldsymbol{\Theta}}\right]^T \Delta\boldsymbol{\Theta}, \tag{28}$$

where $\Delta\dot{V}(s(t))$ and $\Delta\boldsymbol{\Theta}$ are the changes in $\dot{V}(s(t))$ and $\boldsymbol{\Theta}$, respectively. Using the chain rule, obtained:

$$\frac{\partial \dot{V}(s(t))}{\partial \boldsymbol{\Theta}} = \frac{\partial \dot{V}(s(t))}{\partial y^q_{T2FCMAC}} \frac{\partial y^q_{T2FCMAC}}{\partial \boldsymbol{\Theta}} = \frac{\partial s(t)\dot{s}(t)}{\partial y^q_{T2FCMAC}} \frac{\partial y^q_{T2FCMAC}}{\partial \boldsymbol{\Theta}}. \tag{29}$$

Then

$$\frac{\partial \dot{V}(s(t))}{\partial \boldsymbol{\Theta}} = -s(t)\frac{\partial y^q_{T2FCMAC}}{\partial \boldsymbol{\Theta}} = -\frac{1}{2}s(t)\mathbf{F}_{\boldsymbol{\Theta}}(t). \tag{30}$$

From (17)-(23), we obtained

$$\Delta\boldsymbol{\Theta} = -\eta_{\Theta}\frac{\partial s(t)\dot{s}(t)}{\partial \boldsymbol{\Theta}} = \frac{1}{2}\eta_{\Theta}s(t)\mathbf{F}_{\boldsymbol{\Theta}}(t), \tag{31}$$

where η_{Θ} is expressed in terms of $\eta_{\bar{\phi}}$, $\eta_{\underline{\phi}}$, η_o, $\eta_{\bar{\nu}}$, $\eta_{\underline{\nu}}$, η_ω, and η_γ in (16)-(22).
Incorporating (31) and (32) into (30), obtained:

$$\begin{aligned}\Delta\dot{V}(s(t)) &= \left[\frac{\partial \dot{V}(s(t))}{\partial \boldsymbol{\Theta}}\right]^T \Delta\boldsymbol{\Theta} \\ &= \frac{1}{4}\left[-s(t)\mathbf{F}_{\boldsymbol{\Theta}}(t)\right]^T \eta_{\boldsymbol{\Theta}} s(t)\mathbf{F}_{\boldsymbol{\Theta}}(t) \\ &= \frac{1}{4}\left(-s(t)\right)^2 \eta_{\boldsymbol{\Theta}}\mathbf{F}_{\boldsymbol{\Theta}}(t).\end{aligned} \tag{32}$$

From (32), if $\eta_{\boldsymbol{\Theta}}$ is chosen as a positive value, then $\Delta\dot{V}(s(t)) < 0$. Consequently, the Lyapunov stability theorem can guarantee the proposed T2FJCMAC control system's stability. □

4 Results and discussion

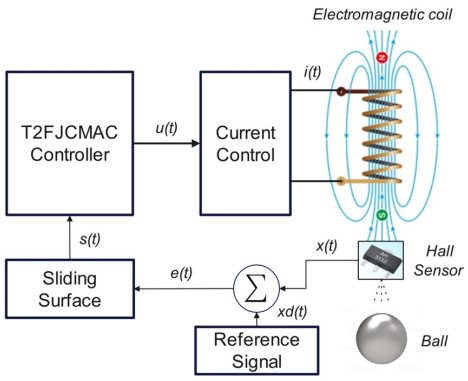


Figure 2: The developed T2FJCMAC network architecture.

The mathematical equations describing the magnetic levitation ball system, as illustrated in Fig. 2, are as follows:

$$Ma = F(x, I) - Mg_m, \tag{33}$$

where:

$$F(x,I) = \frac{\mu_0 N^4 I^2 S}{8}\left((x+h)\ln\left|\frac{R_2+\sqrt{R_2^2+(x+h)^2}}{R_1+\sqrt{R_1^2+(x+h)^2}}\right| + x\ln\left|\frac{R_1+\sqrt{R_1^2+x^2}}{R_2+\sqrt{R_2^2+x^2}}\right|\right),$$

where M denotes the mass of the iron ball, and x indicates the separation between the ball and the magnet. The parameters a and g_m represent the acceleration and the ball's gravitational acceleration, respectively. I denotes the electric current, and F indicates the magnetic force that is being controlled. The symbols μ_0 and h stand for the vacuum permeability and the length of the magnetic coil. Additionally, N is the rotational speed (in revolutions per meter), and S is the area of the magnetic field's cross-section. Lastly, $R1$ and $R2$ are used to represent the maximum and minimum radius of the magnetic coil, respectively.

Based on equation (30), we derive:

$$\ddot{x} = \mathbf{g}(x)u(t) + d. \tag{33}$$

$$\mathbf{g}(x) = \frac{\mu_0 N^4 S}{8M}\left((x+h)\ln\left|\frac{R_2+\sqrt{R_2^2+(x+h)^2}}{R_1+\sqrt{R_1^2+(x+h)^2}}\right| + x\ln\left|\frac{R_1+\sqrt{R_1^2+x^2}}{R_2+\sqrt{R_2^2+x^2}}\right|\right),$$

$$\text{and } u(t) = I^2, \quad d = -g_m.$$

4.1 Simulation results

The simulation results of MLS were performed to evaluate the performance and stability of the system under specific design parameters. The parameters of the MLS system were selected as follows: number of coils $N = 2850$, inner radius $R = 0.012$ m, outer radius $R = 0.038$ m, cross-sectional area $S = 0.0005515$ m^2, permeability of vacuum $= 4 \times 10$ Wb/Am, mass of the ball $M = 0.0216$ kg and gravitational acceleration $g = 9.8$ m/s^2. The simulation program was implemented on Matlab software, using a computer with Core i7 1355U CPU and 16GB RAM. The simulation results show the control efficiency and response-ability of the system under the set conditions, thereby providing a basis for evaluating and improving control methods for the MLS system.
The initial position of the ball is set at -2 mm relative to the equilibrium position. The study is conducted on three main cases: (1) controlling the ball to balance at 0 mm, (2) controlling the ball to track a sinusoidal reference signal, and (3) tracking a sinusoidal reference signal with noise and disturbances. The first case aims to test the stability and position retention of the system under the influence of initial disturbances, while the second case evaluates the tracking and response of the system to the dynamic signal, thereby determining the effectiveness of the proposed control method. Finally, the third case further assesses the controller's robustness by introducing noise and disturbances, evaluating its ability to maintain accurate tracking performance under real-world uncertainties. The random noise is generated using the *randn*() function in MATLAB, which produces random numbers following a normal (Gaussian) distribution with a mean of 0 and a standard deviation of 1. Additionally, disturbances are applied intermittently at fixed time intervals, simulating sudden external effects on the system. This setup ensures that the controller is tested under varying and unpredictable conditions, highlighting its ability to adapt and maintain stability.

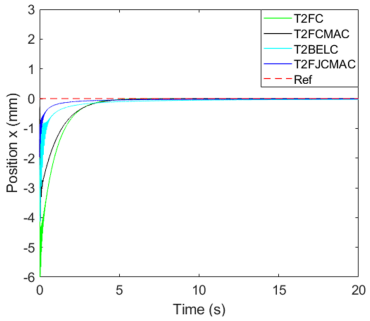


Figure 3: The position of the ball for Case 1.

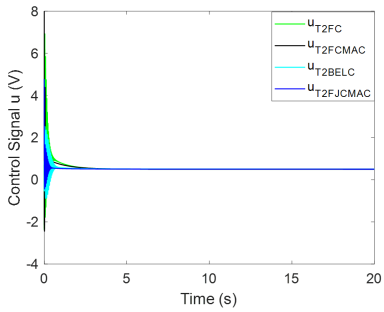


Figure 4: The control signal for Case 1.

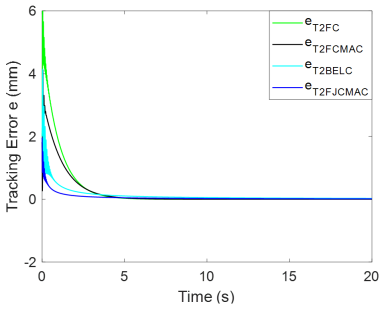


Figure 5: The tracking error system for Case 1.

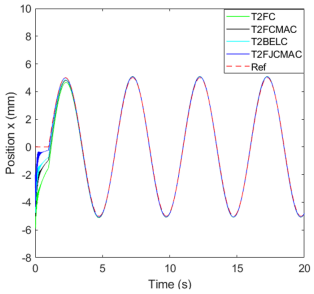


Figure 6: The position of the ball for Case 2.

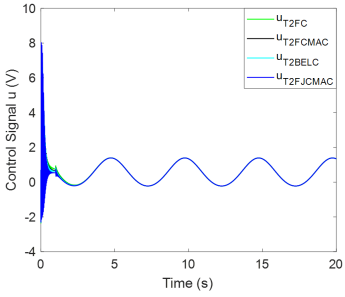


Figure 7: The control signal for Case 2.

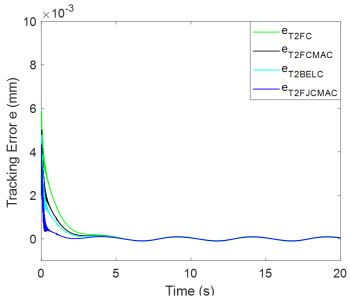


Figure 8: The tracking error system for Case 2.

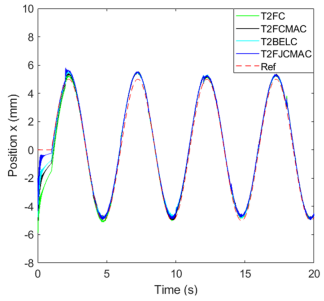


Figure 9: The position of the ball for Case 3.

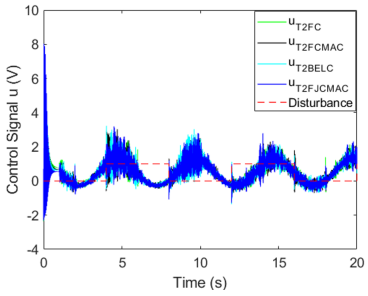


Figure 10: The control signal for Case 3.

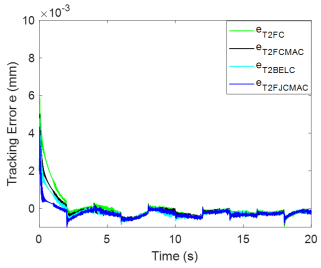


Figure 11: The tracking error system for Case 3.

Figure 3 shows the position of the ball when using the proposed T2FJCMAC controller for Case 1, where the ball is kept balanced at 0 mm. The results show that the control system is capable of stabilizing the position of the ball, with the oscillations quickly decreasing to the equilibrium position after the control force is applied. Figure 4 illustrates the corresponding control signal, showing that the control signal responds promptly to the system fluctuations to maintain the balance. Figure 5 presents the tracking error of the system in Case 1, showing that the tracking error is significantly reduced to near zero after a short period of time, demonstrating the effectiveness of the T2FJCMAC controller in maintaining the stability of the system.
In Case 2, Figure 6 depicts the position of the ball when tracking the sinusoidal reference signal. The results show that the ball follows the reference trajectory with high accuracy, demonstrating the controller's ability to respond flexibly to time-varying signals. Figure 7 shows the control signal in Case 2, showing the appropriate adjustments to ensure that the ball follows the desired trajectory. Figure 8 shows the tracking error of the system in Case 2, with small and stable errors, demonstrating the ability to accurately and efficiently adjust the T2FJCMAC controller in a dynamic environment.
In Case 3, Figure 9 presents the position of the ball when tracking the sinusoidal reference signal under noise and disturbances. The results indicate that despite the presence of external uncertainties, the ball maintains close adherence to the reference trajectory, proving the robustness of the proposed controller. Figure 10 illustrates the corresponding control signal, showing adaptive adjustments to counteract disturbances and maintain accurate tracking. Figure 11 shows the tracking error of the system in Case 3, demonstrating that while minor deviations occur due to noise, the controller effectively mitigates their impact, ensuring stable and precise tracking performance.
The simulation results show that the proposed T2FJCMAC controller provides superior control performance compared to the Type-2 Fuzzy Controller (T2FC), Type-2 Fuzzy CMAC Controller (T2FCMAC), and Type-2 Brain Emotional Learning Controller (T2BELC) in all cases. The proposed T2FJCMAC controller exhibits a faster response, with shorter settling time and smaller oscillations than the other methods. This demonstrates the flexibility and adaptability of the proposed controller in handling dynamic and uncertain signals of the nonlinear system. The comparison of the root mean square error (RMSE) between the controllers, as shown in Table I, shows that the T2FJCMAC controller has the smallest RMSE in all cases. This demonstrates the accurate and efficient trajectory tracking ability of the proposed control method when compared to the T2FC and T2FCMAC methods. This result demonstrates that the combination of Jordan neural network structure and T2FCMAC has brought significant performance advantages, especially in minimizing tracking errors and improving system stability. Thus, the T2FJCMAC controller not only improves the response speed but also ensures better control efficiency in both studied cases. This confirms the superiority of the proposed method in controlling complex nonlinear systems such as magnetic suspension systems.

Table 1: TABLE I
THE RMSE COMPARISON FOR Magnetic Levitation System

	Computation time (ms)	***Case 1***	***Case 2***	***Case 3***
T2FC	0.2638	0.8024	0.6652	0.7010
T2FCMAC	0.3192	0.5504	0.4548	0.5126
T2BELC	0.3725	0.3143	0.3795	0.4650
T2FJCMAC (Proposed method)	0.3437	0.1340	0.2275	0.3804

4.2 Experimental results

The MLS experimental system is constructed as shown in Figure 12, including main components such as electromagnetic coils, position sensors, and a control system connected to a computer to perform control experiments. The proposed control algorithm is implemented on the Arduino R3, which features an ATmega328P microcontroller, 32 KB of flash memory, 2 KB of SRAM, and 1 KB of EEPROM. The clock speed of the Arduino R3 is 16 MHz. A Hall sensor is used for measurement, providing real-time feedback. Communication between the Arduino and external devices is established via UART. Data collection and visualization are performed using MATLAB. The sampling rate of the A/D converter is 10 kHz, and the control sampling time is set to 0.01 ms The experimental results are

conducted to verify the effectiveness of the proposed T2FJCMAC controller in the simulation. The experimental results are evaluated through two main cases.

Case 1, controlling the ball balance at position 0 mm, is presented in Figures 13 to 15. Specifically, Figure 10 shows the position of the ball when using the T2FJCMAC controller for Case 1, showing the good stability of the system in maintaining the balance position with small errors. Figure 11 describes the applied control signal, demonstrating the flexible and timely adjustment of the controller to changes in the system. Figure 12 shows the tracking error of the system, showing that the error level is maintained at a very low level, consistent with the results recorded in the simulation.

For Case 2, the ball control follows the sinusoidal waveform reference signal. In this case, the weight of the ball is also increased to introduce uncertainty and demonstrate the adaptability of the proposed controller. The results show that despite the variation in system dynamics, the controller effectively adjusts its parameters in real-time, maintaining accurate tracking performance and stability. The results are shown from Figure 16 to Figure 18. Figure 16 illustrates the position of the ball, demonstrating the ability to track the reference signal with high accuracy, consistent with the design requirements. Figure 17 depicts the control signal, showing reasonable fluctuations during the tracking of the reference trajectory. Figure 18 shows the tracking error in Case 2, with a small and stable error, confirming the superior performance of the T2FJCMAC controller when applied in real conditions.

These experimental results confirm the feasibility and high efficiency of the T2FJCMAC controller, not only in simulation but also in real environment, well meeting the requirements of stable and accurate control.

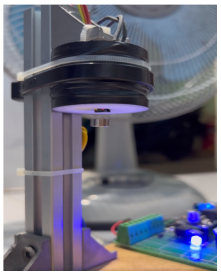


Figure 12: The MLS experimental system.

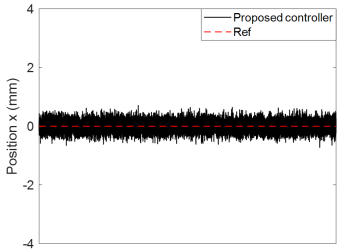


Figure 13: The position of the ball using the proposed T2FJCMAC controller for Case 1 experimental.

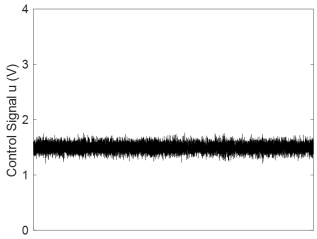


Figure 14: The control signal using the proposed T2FJCMAC controller for Case 1 experimental.

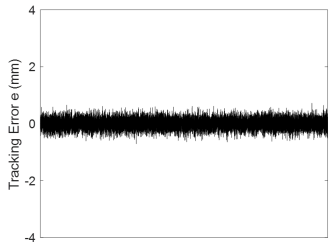


Figure 15: The tracking error system for Case 1 experimental.

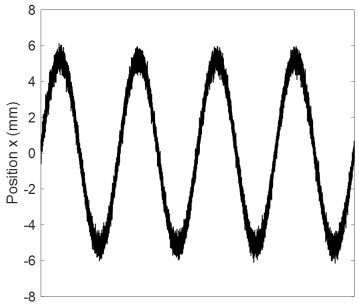


Figure 16: The position of the ball using the proposed T2FJCMAC controller for Case 2 experimental.

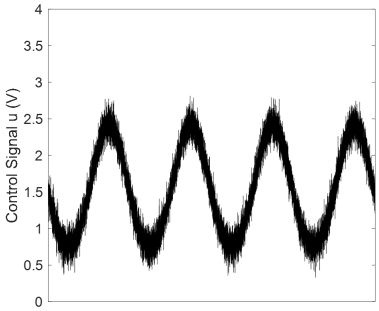


Figure 17: The control signal using the proposed T2FJCMAC controller for Case 2 experimental.

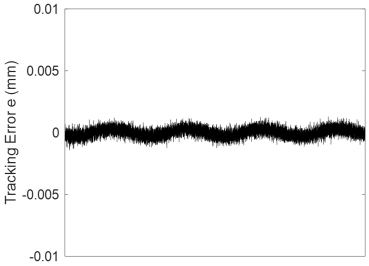


Figure 18: The tracking error system for Case 2 experimental.

5 Conclusions

This study proposed and successfully implemented the T2FJCMAC controller combined with the Jordan neural network to solve the nonlinear control problem of the magnetic suspension system. The simulation and experimental results demonstrated that the proposed method not only significantly improved the accuracy but also enhanced the stability and resilience of the system under the influence of uncertainties and dynamic reference signals. The experimental results showed that this control method is not only suitable for the magnetic suspension system but also has the potential for wide application in other complex nonlinear systems where high requirements for flexibility and control accuracy are required. The improvements in the learning and adaptive capabilities of the controller have confirmed the feasibility of applying advanced techniques to practical control problems. Future research directions will focus on optimizing the structure of the T2FJCMAC controller to minimize the computation time and improve the real-time learning ability. In addition, the research will also extend the application of this method to other nonlinear control systems such as robots, mechatronic systems, and industrial processes that require high precision. However, the proposed method is limited by the learning rate selection, as a large value may cause instability while a small one slows convergence. The current choice is empirically tuned and may not be optimal. Future work could explore adaptive strategies for improved performance.

Acknowledgement

This work was supported by Lac Hong University, Vietnam under grant LHU-RF-TE-23-11-03.

References

[1] M. Abdollahzadeh, M. Pourgholi, *Adaptive fuzzy sliding mode control of magnetic levitation system based on interval type-2 fuzzy neural network identification with an extended Kalman–Bucy filter*, Engineering Applications of Artificial Intelligence, **130** (2024), 10764. https://doi.org/10.1016/j.engappai.2023.107645

[2] J. S. Albus, *A new approach to manipulator control: The cerebellar model articulation controller (CMAC)*, Journal of Dynamic Systems, Measurement, and Control, **97**(3) (1975), 220-227. https://doi.org/10.1115/1.3426922

[3] K. N. Badri, M. Sreekumar, *Diagnosing of risk state in subsystems of CNC turning center using interval type-2 fuzzy logic system with semi elliptic membership functions*, International Journal of Fuzzy Systems, **78**(3) (2021), 1-18. https://doi.org/10.1007/s40815-021-01172-0

[4] J. Bilski, J. Smolag, *Parallel approach to learning of the recurrent Jordan neural network*, Artificial Intelligence and Soft Computing, 12th International Conference, ICAISC 2013, Zakopane, Poland, **I**(12) (2013), 32-40. https://doi.org/10.1007/978-3-642-38658-9_3

[5] F. Chao, D. Zhou, C. M. Lin, C. Zhou, M. Shi, D. Lin, *Fuzzy cerebellar model articulation controller network optimization via self-adaptive global best harmony search algorithm*, Soft Computing, **22**(10) (2018), 3141-3153. https://doi.org/10.1007/s00500-017-2864-4

[6] D. Das, A. K. Das, A. R. Pal, S. Jaypuria, D. K. Pratihar, G. G. Roy, *Meta-heuristic algorithms-tuned Elman vs. Jordan recurrent neural networks for modeling of electron beam welding process*, Neural Processing Letters, **53** (2021), 1647-1663. https://doi.org/10.1007/s11063-021-10471-4

[7] S. Dey, S. Banerjee, J. Dey, *Practical application of fractional-order PID controller based on evolutionary optimization approach for a magnetic levitation system*, IETE Journal of Research, **69**(11) (2022), 8168-8192. https://doi.org/10.1080/03772063.2022.2052983

[8] A. M. El-Nagar, M. El-Bardini, A. A. Khater, *A class of general type-2 fuzzy controller based on adaptive alpha-plane for nonlinear systems*, Applied Soft Computing, **133** (2023), 109938. https://doi.org/10.1016/j.asoc.2022.109938

[9] M. Ghasemi, M. Kelarestaghi, F. Eshghi, A. Sharifi, *T2-FDL: A robust sparse representation method using adaptive type-2 fuzzy dictionary learning for medical image classification*, Expert Systems with Applications, **158** (2020), 113500. https://doi.org/10.1016/j.eswa.2020.113500

[10] S. M. Hosseini, M. Manthouri, *Type 2 adaptive fuzzy control approach applied to variable speed DFIG based wind turbines with MPPT algorithm*, Iranian Journal of Fuzzy Systems, **9**(1) (2022), 31-45. https://doi.org10.22111/ijfs.2022.6549

[11] S. Karagöz, M. Deveci, V. Simic, N. Aydin, *Interval type-2 fuzzy ARAS method for recycling facility location problems*, Applied Soft Computing, **102** (2021), 107107. https://doi.org/10.1016/j.asoc.2021.107107

[12] A. Karuppannan, M. Muthusamy, *Wavelet neural learning-based type-2 fuzzy PID controller for speed regulation in BLDC motor*, Neural Computing and Applications, **33** (2021), 13481-13503. https://doi.org/10.1007/s00521-021-05971-2

[13] A. Kumar, R. Raj, P. Gaidhane, O. Castillo, *Artificial bee colony optimized precompensated interval type-2 fuzzy logic controller for a magnetic levitation system*, Recent Trends on Type-2 Fuzzy Logic Systems: Theory, Methodology and Applications, Springer, (2023), 43-56. https://doi.org/10.1007/978-3-031-26332-3_4

[14] S. Kumari, S. Aravindakshan, U. Jain, V. C. Srinivasa, *Convolutional elman Jordan neural network for reconstruction and classification using attention window*, Innovations in Computational Intelligence and Computer Vision: Proceedings of ICICV 2020, Springer, (2021), 173-181. https://doi.org/10.1007/978-981-15-6067-5_20

[15] T. L. Le, N. V. Quynh, S. K. Hong, *Multilayer interval type-2 fuzzy controller design for quadcopter unmanned aerial vehicles using Jaya algorithm*, IEEE Access, **8** (2020), 181246-181257. https://doi.org/10.1109/ACCESS.2020.3028617

[16] C. M. Lin, M. S. Yang, F. Chao, X. M. Hu, J. Zhang, *Adaptive filter design using type-2 fuzzy cerebellar model articulation controller*, IEEE Transactions on Neural Networks and Learning Systems, **27**(10) (2016), 2084-2094. https://doi.org/10.1109/TNNLS.2015.2491305

[17] S. Lv, Z. Li, J. Huang, P. Shi, *A novel interval type-2 fuzzy classifier based on explainable neural network for surface electromyogram gesture recognition*, IEEE Transactions on Human-Machine Systems, **53**(6) (2023), 955-64. https://doi.org/10.1109/THMS.2023.3310524

[18] M. Manceur, N. Essounbouli, A. Hamzaoui, *Second-order sliding fuzzy interval type-2 control for an uncertain system with real application*, Transactions on Fuzzy Systems, **20**(2) (2012), 262-275. https://doi.org/10.1109/TFUZZ.2011.2172948

[19] S. Mobayen, A. N. Vargas, L. Acho, G. Pujol-Vázquez, D. F. Caruntu, *Stabilization of two-dimensional nonlinear systems through barrier-function-based integral sliding-mode control: Application to a magnetic levitation system*, Nonlinear Dynamics, **111**(2) (2023), 1343-1354. https://doi.org/10.1007/s11071-022-07890-w

[20] A. Mohammadzadeh, C. Zhan, K. A. Alattas, F. F. El-Sousy, M. T. Vu, *Fourier-based type-2 fuzzy neural network: Simple and effective for high dimensional problems*, Neurocomputing, **547** (2023), 126316. https://doi.org/10.1016/j.neucom.2023.126316

[21] A. K. Sahoo, S. K. Mishra, D. S. Acharya, S. Chakraborty, S. K. Swain, *A comparative evaluation of a set of bio-inspired optimization algorithms for design of two-DOF robust FO-PID controller for magnetic levitation plant*, Electrical Engineering, **105**(5) (2023), 3033-3054. https://doi.org/10.1007/s00202-023-01867-7

[22] A. Salimi-Badr, M. Hashemi, H. Saffari, *A type-2 neuro-fuzzy system with a novel learning method for Parkinson's disease diagnosis*, Applied Intelligence, **53**(12) (2023), 15656-15682. https://doi.org/10.1007/s10489-022-04276-8

[23] M. A. Seto, A. Ma'arif, *PID control of magnetic levitation (Maglev) system*, Journal of Fuzzy Systems and Control, **1**(1) (2023), 25-27. https://doi.org/10.59247/jfsc.v1i1.28

[24] L. Su, X. Ling, *Estimating weak pulse signal in chaotic background with Jordan neural network*, Complexity, **2020**(1) (2020), 3284587. https://doi.org/10.1155/2020/3284587

[25] D. Sundaram, *Controllability criteria for type-2 fuzzy fractional-order dynamical system via mittag-leffler matrix function using granular derivative*, Iranian Journal of Fuzzy Systems, **21**(5) (2024), 133-150. https://doi.org/10.22111/ijfs.2024.47862.8422

[26] J. Tang, Z. Huang, Y. Zhu, J. Zhu, *Neural network compensation control of magnetic levitation ball position based on fuzzy inference*, Scientific Reports, **12**(1) (2022), 1795. https://doi.org/10.1038/s41598-022-05900-w

[27] C. Urrea, C. Domínguez, J. Kern, *Modeling, design and control of a 4-arm delta parallel manipulator employing type-1 and interval type-2 fuzzy logic-based techniques for precision applications*, Robotics and Autonomous Systems, **175** (2024), 104661. https://doi.org/10.1016/j.robot.2024.104661

[28] P. Verma, R. Garg, P. Mahajan, *Asymmetrical interval type-2 fuzzy logic control based MPPT tuning for PV system under partial shading condition*, ISA Transactions, **100** (2020), 251-263. https://doi.org/10.1016/j.isatra.2020.01.009

[29] P. Vernekar, V. Bandal, *Sliding mode control for magnetic levitation systems with mismatched uncertainties using multirate output feedback*, International Journal of Dynamics and Control, **11**(6) (2023), 2958-2976. https://doi.org/10.1007/s40435-023-01151-3

[30] A. T. Vo, T. N. Truong, H. J. Kang, T. D. Le, *A fixed-time sliding mode control for uncertain magnetic levitation systems with prescribed performance and anti-saturation input*, Engineering Applications of Artificial Intelligence, **133** (2024), 108373. https://doi.org/10.1016/j.engappai.2024.108373

[31] C. L. Zhang, X. Z. Wu, J. Xu, *Particle swarm sliding mode-fuzzy PID control based on maglev system*, IEEE Access, **9** (2021), 96337-96344. https://doi.org/10.1109/ACCESS.2021.3095490